

# The method of finite spheres

S. De, K. J. Bathe

**Abstract** The objective of this paper is to present some of our recent developments in meshless methods. In particular, a technique is given – the method of finite spheres – that is truly meshless in nature in the sense that the nodes are placed and the numerical integration is performed without a mesh. The method can be viewed as a special case of the general formulation known as the meshless local Petrov–Galerkin (MLPG) procedure. Some of the novel features of the method of finite spheres are the numerical integration scheme and the way in which the Dirichlet boundary conditions are incorporated. A new way of modeling doubly-connected domains is also presented. Various example problems are solved to demonstrate the method.

## List of symbols

$A$	Interior of a set in $R^n$ , $n = 1, 2, 3$ .
$\partial A$	Boundary of set $A$
$\bar{A}$	$= A \cup \partial A$ Closure of set $A$
$\text{supp}(v)$	$= \{\mathbf{x} \in A; v(\mathbf{x}) \neq 0\}$ Support of a function $v$
$\Omega$	Open bounded domain in $R^n$ , $n = 1, 2, 3$ .
$\Gamma$	$= \partial\Omega$ Boundary of $\Omega$ (assumed to be Lipschitz continuous)
$\mathbf{n}$	Outward unit normal defined on $\Gamma$
$B(\mathbf{x}_I, r_I)$	$= \{\mathbf{x} \in A; \ \mathbf{x} - \mathbf{x}_I\ _0 < r_I\}$ Open sphere of radius $r_I$ centered at $\mathbf{x}_I$ in $n$ -dimensional Euclidean space ( $n = 1, 2$ or $3$ )
$S(\mathbf{x}_I, r_I)$	$= \{\mathbf{x} \in A; \ \mathbf{x} - \mathbf{x}_I\ _0 = r_I\}$ Surface of the $n$ -dimensional sphere of radius $r_I$ centered at $\mathbf{x}_I$ .
$h$	a global measure of the support radii (determined by the values of $r_I$ )
$h_{Im}(\mathbf{x})$	$=$ The $m$ th shape function at node $I$
$C^m(A)$	Space of functions with continuous derivatives up to order $m$ on $A$

$C_0^m(A)$	$= \{v   v \in C^m(A); \text{supp}(v) \text{ is a compact subset of } A\}$
$Q_m(A)$	Space of polynomials of degree $\leq m$ defined on $A$
$V^{h,p}$	The two-parameter global approximation space (depending on parameters $h$ and $p$ ).
$v^{h,p} \in V^{h,p}$	
$a(\cdot, \cdot)$	A bilinear form from $V^{h,p} \times V^{h,p} \mapsto R$
$V_I^{h,p}$	The two-parameter local approximation space.
$v_I^{h,p} \in V_I^{h,p}$	

## 1 Introduction

In spite of the great success of the finite element method and the closely related finite volume method as effective numerical tools for the solution of boundary value problems on complex domains, there has been a growing interest in the so-called “meshless” methods over the past decade. A number of methods have been proposed so far including the smooth particle hydrodynamics (SPH) method (Monaghan, 1988), the diffuse element method (DEM) (Nayroles et al., 1992), the element free Galerkin (EFG) method (Belytschko et al., 1994), the reproducing kernel particle method (RKPM) (Liu et al., 1993), the moving least-squares reproducing kernel method (MLSRK) (Li and Liu, 1996; Liu et al., 1997) the partition of unity finite element method (PUFEM) (Melenk, 1992; Melenk and Babuška, 1996; Babuška and Melenk, 1997; Melenk and Babuška, 1997), the hp-clouds method (Duarte and Oden, 1996a; Duarte and Oden 1996b), the reproducing kernel hierarchical partition of unity method (Li and Liu, 1999a, b), the finite point method (Oñate et al., 1996), the local boundary integral equation (LBIE) method (Zhu et al., 1998b) and the meshless local Petrov–Galerkin (MLPG) method (Atluri et al., 1999a, b; Atluri and Zhu 1998a, b).

The primary reason for the interest in meshless methods is that in the finite element/finite volume method a mesh is required. The automatic generation of good quality meshes presents significant difficulties in the analysis of engineering systems (especially in three dimensions) and these difficulties are circumvented when no mesh is needed.

The established computational methods which are based on the weighted residual technique have three key ingredients:

*Interpolation:* An expansion of the unknown field variable/s in terms of trial basis/shape functions and unknown parameters,

Received 26 October 1999

S. De, K. J. Bathe (✉)  
Department of Mechanical Engineering,  
Massachusetts Institute of Technology,  
77 Massachusetts Avenue,  
Cambridge, MA 02139, USA

The authors would like to thank Dr. M.A. Srinivasan of the Research Laboratory of Electronics, M.I.T. for the support of this work, and Professors S.N. Atluri, I. Babuška, T. Belytschko, W.K. Liu and J.T. Oden for their comments on an earlier version of this paper.

*Integration:* The determination of the governing algebraic equations by setting the residual error orthogonal to a set of test functions which may or may not coincide with the trial functions, and

*Solution of the algebraic equations:* The solution of the governing equations for the unknown parameters.

If the first two steps can be performed without a mesh, then what results is a “truly meshless” method. Many of the early “meshless” techniques such as the DEM, EFGM, *hp*-clouds method etc. are not truly meshless since even if the interpolation is independent of a background mesh, the integration is not.

In the finite element/finite volume methods the interpolation functions are polynomials (or mapped polynomials) and the numerical integration is performed most efficiently using Gauss-Legendre product rules on  $n$ -dimensional cubes or tetrahedra (in the mapped isoparametric space). Failure to perform the integration accurately results in loss of accuracy and possibly stability of the solution scheme (Bathe, 1996). In most mesh-free techniques, however, complicated non-polynomial interpolation functions are used which render the integration of the weak form rather difficult (Dolbow and Belytschko, 1999).

Another difficulty lies in the accurate imposition of the Dirichlet boundary conditions. The Kronecker delta property of the finite element/finite volume shape functions allows the incorporation of these conditions very efficiently (Bathe, 1996). But the interpolation functions used in most meshless schemes do not satisfy this condition at the nodes and hence the imposition of Dirichlet boundary conditions becomes complicated. Popular with researchers are techniques involving Lagrange multipliers (Belytschko, 1994), penalty formulations (Atluri and Zhu, 1998a, b), use of finite elements along Dirichlet boundaries (Krongauz and Belytschko, 1996), modified variational principles (Lu et al., 1994), corrected collocation techniques (Wagner and Liu, 1999) and transformation methods (Atluri et al., 1999a).

A survey of meshless techniques may be found in Duarte (1995) and Belytschko et al. (1996). The major meshless methods described in these two review works, namely the RKPM, SPH method, DEM and EFG method are based on three classes of interpolation functions: wavelets, moving least squares functions (used in the DEM and the EFG method), and the partition of unity (PU) or *hp*-clouds functions (used in the PUFEM and *hp*-clouds methods). All these methods are really “pseudo meshless” since they use a background mesh for the numerical integration (and sometimes even for imposing the Dirichlet boundary conditions).

The finite point method (Oñate et al., 1996) is a truly meshless scheme. The method uses a weighted least squares (WLS) interpolation and point collocation, thus bypassing integration. However, methods based on point collocation are notorious for the sensitivity of the solution on the choice of “proper” collocation points.

As a truly meshless technique, the meshless local Petrov-Galerkin (MLPG) method (Atluri and Zhu, 1998a) seems to be the most promising. The technique is based on a weak form computed over a local sub-domain, which can

be any simple geometry like a sphere, cube or an ellipsoid for ease of integration. The trial and test function spaces can be different or may be the same. Any class of functions with compact support satisfying certain approximation properties (like the MLS functions or PU functions) can be used as trial and test functions (Atluri et al., 1999a). This method has been successfully applied to a wide range of problems (Atluri et al., 1999a, b; Atluri and Zhu, 1998a, b) and is of very general nature. A method using a similar approach but boundary integral techniques is the local boundary integral equation (LBIE) method (Zhu et al., 1998b).

However, although considerable efforts have been made in the development of meshless methods, the currently available techniques are still computationally much less efficient than the well established finite element/finite volume procedures. The primary reason is that complicated (non-polynomial) shape functions are employed and the required numerical integration is very difficult to perform efficiently. Hence some researchers (refer to Oden et al., 1998; Duarte et al., 1999) have reverted back to developing finite element techniques incorporating certain aspects of the meshless methods. In this paper, however, we concentrate attention on methods which are truly meshless and endeavor to make them as efficient as possible.

The objective of this paper is to present some developments using the MLPG approach with the aim of reaching a powerful solution technique. In the method of finite spheres, the MLPG concept is used with a specific choice of geometric sub-domains, test and trial function spaces, numerical integration technique, and a procedure for imposing the essential boundary conditions.

The method of finite spheres uses compactly supported PU functions to form a globally conforming approximation space and a Bubnov-Galerkin formulation as the weighted residual scheme. Figure 1 shows a schematic of the method as a natural generalization of the finite element method. In the classical finite element/finite volume method the support of a shape function corresponding to a node is usually a polytope in  $n$ -dimensions whereas the method of finite spheres uses  $n$ -spheres as supports. Integration is performed on the  $n$ -dimensional spheres or spherical shells using specialized cubature rules.

A brief outline of the paper is as follows. In Sect. 2 we discuss in detail our justification for the use of PU basis functions based on Shepard partitions of unity and summarize key results relating to consistency and a-priori error analysis. In Sect. 3 we derive the weak form for a symmetric second-order differential operator. In Sect. 4 we discuss the imposition of Neumann and Dirichlet boundary conditions. Even though we primarily concentrate on the  $n$ -dimensional sphere as our integration domain, we realize that to deal with doubly-connected domains efficiently, the ideas of support and integration domain have to be decoupled. To address the solution of such problems we present, in Sect. 5, our developments using  $n$ -dimensional spherical shells. In Sect. 6 we deal with issues related to numerical integration on the  $n$ -dimensional spheres and spherical shells. Finally, in Sect. 7, several numerical solutions are provided to demonstrate the method of finite spheres.

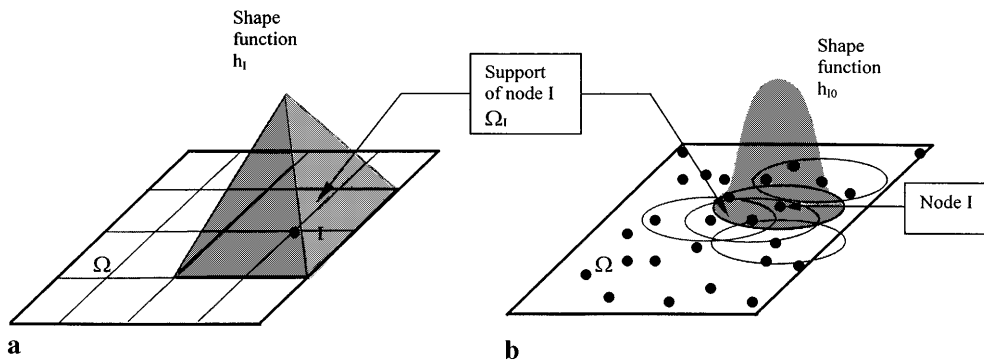


Fig. 1a, b. Discretization of a domain  $\Omega$  in  $\mathbb{R}^2$  by the finite element method (a) and the method of finite spheres (b). In (a) the domain is discretized by quadrilateral elements with a node at each vertex point. The finite element shape function  $h_I$  is shown at node I. In (b) the domain is discretized using a set of nodes only. Corresponding to each node I, there is a sphere (i.e. a disk in  $\mathbb{R}^2$ ), centered at the node, which is the support of a set of shape functions corresponding to that node. One such shape function,  $h_{I0}$ , is shown in the figure

## 2

### The interpolation scheme

The first step in the Bubnov–Galerkin procedure is to construct finite dimensional subspaces  $V_i$  of a Sobolev space, in which the weak solution is assumed to exist. In a large variety of practical applications, namely, problems associated with second-order partial differential operators, the Sobolev space under consideration is  $H^1(\Omega)$ , the first-order Hilbert space. We summarize the theory in that setting, extension to higher-order spaces can be achieved. We are interested in approximation spaces which satisfy the following minimal requirements:

**Consistency or polynomial reproducing property** The consistency condition is related to the degree of the governing partial differential equation. For example, when solving an elasticity problem using a displacement-based formulation, the approximating functions should not only be able to reproduce constant functions (the so-called “rigid body” modes) but also linear functions (the “constant strain” states), i.e., we look for at least first-order consistency. Thus, we should be able to reproduce polynomials to a certain order to satisfy the consistency requirement.

**Local approximability** This is a more general requirement than just consistency and is related to the reproducing properties of the trial functions. If we know the nature of the solution in certain subdomains of  $\Omega$ , we should be able to incorporate specific functions in the global approximation space in order to enrich this space to closely represent the solution. There are certain situations where singularities arise naturally in the solution of the governing differential equations and polynomials perform poorly in resolving such singularities. The idea is to use available analytical solutions to improve numerical predictions.

**Continuity** The approximation functions should satisfy certain minimal continuity conditions.

**Localization by compact support** One of the major reasons of the success of the finite element procedure is the concept of approximations using piece-wise polynomials

on compactly supported domains (elements). The main advantages of using compactly supported functions, i.e. functions that are nonzero only on small subsets of  $\Omega$ , are that (1) they allow the localization of the approximation (and hence steep gradients can be handled by using more functions locally), (2) they result in banded system matrices since only a few of the supports overlap at any given point of the domain and (3) they allow a natural means of controlling the rate of convergence of numerical schemes through  $h$ ,  $p$  or  $hp$ -type refinements.

There is no unique way of constructing the approximation spaces. The current interest in the so-called meshless methods has been primarily spurred by the ability to construct non-polynomial approximation spaces with compact support without the need for a background mesh. As we mentioned already, examples of such approximation functions are compactly supported wavelet functions, the MLS (moving least squares) functions (Nayroles et al., 1992; Belytschko et al., 1994), the PU functions of Babuška and Melenk (Melenk and Babuška, 1996) and the  $hp$ -cloud functions of Duarte and Oden (Duarte and Oden, 1996a, b). In the wavelet-based methods, compactly supported functions with desirable properties are developed using FIR (finite impulse response) filter-banks. The difficulties of using wavelets as basis functions are that they are designed to have desirable orthogonality properties in  $L^2(\Omega)$  but not in higher-order Hilbert spaces, the computation of inner products through “connection coefficients” is very cumbersome and the application of wavelets to arbitrary domains is still being researched.

The moving least squares technique of generating compactly supported functions having desirable reproducing properties is quite appealing, but has some drawbacks, most important of which is the need to invert a  $m \times m$  matrix (when  $m$  basis functions are used to generate the MLS shape functions). Besides increasing the computational cost for any  $m > 1$ , this requirement means that at each evaluation point at least  $m$  weight functions should be nonzero for the matrix to be invertible.

Of the existing techniques for the generation of compactly supported basis functions, the methods developed using the partition of unity (PU) paradigm appear to be

the most general. They possess the desirable properties we have listed above and it is possible to generate low-cost partitions of unity (without the need to invert matrices) (Duarte and Oden 1996a). Moreover, the finite element/finite volume basis functions and the MLS basis functions may be looked upon as specialized applications of the partition of unity construction technique.

We have adopted the PU paradigm to generate the shape functions for the method of finite spheres. We briefly summarize the construction of these basis functions and state important results in the following two sections. For details regarding the theory of the PU method as well as for proofs of the theorems see Melenk (1992), Melenk and Babuška (1996), Duarte and Oden (1996a).

## 2.1

### The partition of unity functions

The first step in the PU method is of course the generation of the partition of unity functions.

**Definition 2.1** Let  $\Omega \in R^n$  ( $n = 1, 2, 3$ ) be an open bounded domain. Let a family of open sets  $\{\Omega_I; I = 1, 2, \dots, N, N = N(h), h > 0\}$  form a covering for  $\Omega$ , i.e.,  $\Omega \subset \bigcup_{I=1}^N \Omega_I$ . Then there exists a system of functions  $\{\phi_I\}_{I=1}^N$  of  $C_0^s(R^n)$ ,  $s \geq 0$  such that

1.  $\sum_{I=1}^N \phi_I(\mathbf{x}) \equiv 1 \quad \forall \mathbf{x} \in \Omega$ .
2.  $\text{supp}(\phi_I) \subset \Omega_I$ .

Then this system of functions  $\{\phi_I\}_{I=1}^N$  is defined as a **partition of unity** subordinate to the open cover  $\{\Omega_I\}$  (Yosida, 1978).

The sets  $\{\Omega_I\}$  are also called “clouds” or “patches” (Melenk and Babuška, 1996; Duarte and Oden, 1996a). In the method of finite spheres (MFS) we choose  $\Omega_I \equiv B(\mathbf{x}_I, r_I)$ , which geometrically represents a **sphere**. We associate a “node” with the center,  $\mathbf{x}_I$  ( $I = 1, 2, \dots, N$ ), of each sphere. By  $\Gamma_I$  we denote the surface of the sphere,  $S(\mathbf{x}_I, r_I)$ . We use a particular family of (nonpolynomial) PU functions, called the Shepard partitions of unity (Shepard, 1968) having zeroth-order consistency (i.e., these functions can only reproduce constant functions exactly). Let  $W_I(\mathbf{x})$  denote a weighting function with the following properties:

1.  $W_I(\mathbf{x}) \in C_0^s(R^n)$ ;  $s \geq 0$ .
2.  $\text{supp}(W_I) \subset \Omega_I$ .

The Shepard partition of unity functions are defined as

$$\phi_I^0(\mathbf{x}) = \frac{W_I}{\sum_{J=1}^N W_J} \quad (1)$$

Important considerations in the choice of the weight functions are the continuity class to which they belong and how easily they can be differentiated and integrated. We follow Duarte’s work (Duarte and Oden, 1996a) and choose quartic spline weight functions (which belong to  $C_0^1(\Omega)$ ):

$$W_I(s) = \begin{cases} 1 - 6s^2 + 8s^3 - 3s^4 & 0 \leq s < 1 \\ 0 & s \geq 1 \end{cases}$$

where  $s = (\|\mathbf{x} - \mathbf{x}_I\|_0)/r_I$ .

## 2.2

### The approximation spaces $V^{h,p}$

Having chosen the Shepard functions which satisfy the PU requirement, we are in a position to develop approximation spaces which are subspaces of  $H^1(\Omega)$ . Let  $V_I^{h,p} \subset H^1(\Omega \cap \Omega_I)$  be a two parameter family of function spaces, the parameters being  $h$  (the size of the sphere) and  $p$  (the polynomial order) (Melenk and Babuška, 1996; Duarte and Oden, 1996a), such that

$$Q_p \subset \text{span}(V_I^{h,p}) \quad \forall I$$

then we define the two-parameter global approximation space  $V^{h,p}$  as

$$V^{h,p} = \sum_{I=1}^N \phi_I^0 V_I^{h,p} \subset H^1(\Omega) \quad .$$

Since  $V_I^{h,p} = \text{span}_{m \in \mathcal{J}}(p_m(\mathbf{x}))$ , where  $\mathcal{J}$  is an index set and  $p_m(\mathbf{x})$  is a member of the local basis, any function  $v_I^{h,p} \in V_I^{h,p}$  can be expressed as  $v_I^{h,p}(\mathbf{x}) = \sum_{m \in \mathcal{J}} \alpha_{Im} p_m(\mathbf{x})$ , for  $\alpha_{Im} \in R$ . If we multiply each  $p_m(\mathbf{x})$  by  $\phi_I^0(\mathbf{x})$ , the resulting function has the same support as  $\phi_I^0(\mathbf{x})$ . The global approximation space is constructed using such products. Hence, any function  $v^{h,p} \in V^{h,p}$  can now be written as

$$v^{h,p}(\mathbf{x}) = \sum_{I=1}^N \sum_{m \in \mathcal{J}} h_{Im}(\mathbf{x}) \alpha_{Im} \quad (2)$$

where

$$h_{Im}(\mathbf{x}) = \phi_I^0(\mathbf{x}) p_m(\mathbf{x})$$

and  $h_{Im}$  is a basis/shape function associated with the  $m$ th degree of freedom of node  $I$ . We now state, without proof, some important properties of the discretization scheme (for proofs see Melenk and Babuška, 1996; Duarte and Oden, 1996a). We use the symbol  $C$  to denote a generic positive constant which may take different values at successive occurrences (including in the same equation).

**Theorem 2.1 (Reproducing property).** If any function  $p_m(\mathbf{x})$  is included in the local bases, it is possible to exactly reproduce it.

**Corollary 2.1 (Consistency).** If  $Q_m \subset \text{span}(V_I^{h,p}) \forall I$ , then  $Q_m \subset \text{span}(V^{h,p})$ .

**Theorem 2.2 (Continuity).** Let  $W_I, I = 1, 2, \dots, N \in C_0^s(\Omega_I)$  and let  $p_m(\mathbf{x}) \in C^l(\Omega)$  for  $s, l \geq 0$ ; then the shape functions  $h_{Im}(\mathbf{x})$  satisfy  $h_{Im}(\mathbf{x}) \in C_0^{\min(s,l)}(\Omega_I \cap \Omega)$ .

**Theorem 2.3 (Approximation error estimate).** Let  $u$  be the function to be approximated, and let the given PU functions  $\{\phi_I(\mathbf{x})\}$  satisfy

$$\|\phi_I\|_{L^\infty(R^n)} \leq C \quad ,$$

$$\|\nabla \phi_I\|_{L^\infty(R^n)} \leq \frac{C}{r_I} \quad .$$

Assume that the local approximation spaces  $V_I^{h,p}$  have the following properties: On each patch  $\Omega_I \cap \Omega$ ,  $u$  can be approximated by a function  $v_I^{h,p} \in V_I^{h,p}$  such that

$$\|u - v_I^{h,p}\|_{L^2(\Omega_I \cap \Omega)} \leq \epsilon_1(I, h, p, u) ,$$

$$\|\nabla(u - v_I^{h,p})\|_{L^2(\Omega_I \cap \Omega)} \leq \epsilon_2(I, h, p, u) .$$

then there is a function  $v^{h,p} \in V^{h,p}$  satisfying

$$\|u - v^{h,p}\|_{L^2(\Omega)} \leq C \left( \sum_{I=1}^N (\epsilon_1(I, h, p, u))^2 \right)^{1/2}$$

$$\|\nabla(u - v^{h,p})\|_{L^2(\Omega)} \leq \left( \sum_{I=1}^N \left( \frac{C}{r_I} \right)^2 (\epsilon_1(I, h, p, u))^2 + C(\epsilon_2(I, h, p, u))^2 \right)^{1/2} .$$

**Theorem 2.4 (Convergence rate of the  $h$ -version).** Let  $u \in H^k(\Omega)$ ,  $k \geq 2$ . Let  $V_I^{h,p}$  have the following approximation properties:

$$\epsilon_1(I, h, u) \leq Cr_I^{\mu+1} \|u\|_{H^k(\Omega_I \cap \Omega)}$$

$$\epsilon_2(I, h, u) \leq Cr_I^\mu \|u\|_{H^k(\Omega_I \cap \Omega)}$$

for some appropriate  $\mu > 0$ . If  $u^{h,p}$  is the numerical solution, then

$$\|u - u^{h,p}\|_{L^2(\Omega)} \leq Ch^{\mu+1} \|u\|_{H^k(\Omega)},$$

$$\|\nabla(u - u^{h,p})\|_{L^2(\Omega)} \leq Ch^\mu \|u\|_{H^k(\Omega)} .$$

Theorem 2.1 states that if we include a-priori knowledge of the solution in local subdomains, then this knowledge will enhance the approximation capability because the functions representing this knowledge can be reproduced. Corollary 2.1 assures that it is possible to obtain any order of consistency, at least theoretically. It turns out that for our choice of the PU functions, the functions  $h_{Im}$  are linearly independent, i.e.  $V^{h,p} = \text{span}(h_{Im}(\mathbf{x}))$ , as long as the local bases are linearly independent. Theorem 2.2 tells us what order of continuity is obtained by the global approximation. Theorem 2.3 is of very general nature and provides an interpolation error estimate if the local approximation behavior is known. Theorem 2.4 is an application of the previous theorem to obtain a bound on the solution error. Specifically if a polynomial basis of degree  $p$  is used as the local approximation space, and  $k = p + 1$ , then  $\mu = p$  and an  $\mathcal{O}(h^{p+1})$  convergence in the solution variable is predicted. Duarte and Oden have pointed out that the use of Shepard functions to generate the partitions of unity is probably the least expensive for a given level of accuracy (Duarte and Oden, 1996a).

### 3 The weak form for a $n$ -dimensional sphere

In this section, we develop the weak form and discretized equations of the governing differential equation by integrating over each  $n$ -dimensional sphere centered around a node. We focus on a second-order partial differential equation in a single variable. Extension to multiple variables and higher-order differential operators can be directly achieved.

Consider the operator equation

$$Au = f \quad \text{in } \Omega \quad (3)$$

where  $A: \mathcal{D}_A \subset H^2(\Omega) \mapsto L^2(\Omega)$  is a second-order symmetric positive definite differential operator with domain of definition  $\mathcal{D}_A$  and  $f \in L^2(\Omega)$  is the forcing function, with

$$A = - \sum_{i,j=1}^d \frac{\partial}{\partial x_i} a_{ij}(\mathbf{x}) \frac{\partial}{\partial x_j} + c(\mathbf{x})$$

where  $d$  is the dimensionality of the problem,  $a_{ij}(\mathbf{x})$  and  $c(\mathbf{x})$  are bounded measurable coefficients. Assume that Neumann boundary conditions are prescribed over the boundary  $\Gamma_f$

$$\sum_{i,j=1}^d a_{ij}(\mathbf{x}) \frac{\partial u}{\partial x_j} n_i = f^s \quad \text{on } \Gamma_f \quad (4)$$

where  $n_i$  is the component of the outward unit normal on the boundary along the  $i$ th direction (see Fig. 2), and Dirichlet boundary conditions are provided on the boundary  $\Gamma_u$

$$u = u^s \quad \text{on } \Gamma_u \quad (5)$$

where  $\Gamma = \Gamma_u \cup \Gamma_f$  and  $\Gamma_u \cap \Gamma_f = \emptyset$ . In the Bubnov-Galerkin procedure, we find the approximation  $u^{h,p} \in V^{h,p}$  to the true solution  $u$  by making the residual  $(Au^{h,p} - f)$  orthogonal to the basis functions  $\{h_{Im}\}$ . Hence, corresponding to node  $I$ , we generate the following set of equations:

$$(Au^{h,p} - f, h_{Im}) = 0, \quad m \in \mathcal{I} .$$

Using Eq. (2) and Green's Theorem, we obtain the  $m$ th equation corresponding to the  $I$ th node as

$$\sum_{J=1}^N \sum_{n \in \mathcal{I}} K_{ImJn} \alpha_{Jn} = f_{Im} + \hat{f}_{Im} \quad (6)$$

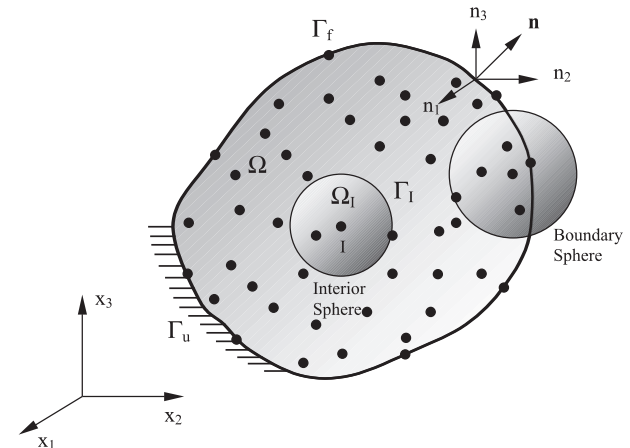


**Fig. 2.** General three-dimensional body discretized using a set of nodes. Associated with each node  $I$  is a sphere  $\Omega_I$ . Spheres that lie completely inside the domain are called “interior spheres” while those which intersect the boundary of the domain,  $\Gamma$ , are called “boundary spheres”. Dirichlet boundary conditions are prescribed over a portion  $\Gamma_u$  of the boundary while Neumann boundary conditions are prescribed over  $\Gamma_f$ ;  $\Gamma = \Gamma_u \cup \Gamma_f$ ,  $\Gamma_u \cap \Gamma_f = \emptyset$

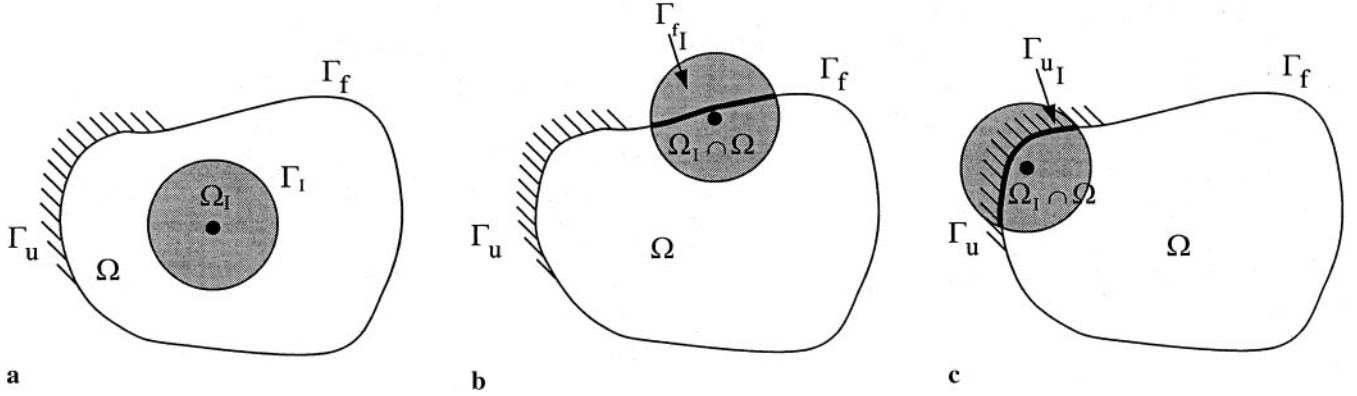


Fig. 3a-c. Figure showing “interior spheres” (a) and “boundary spheres” (b) & (c). Integration is performed on  $\Omega_I$  in (a) and on  $\Omega_I \cap \Omega$  in (b) & (c)

where

$$K_{ImJn} = a(h_{Im}, h_{Jn}) = \int_{\Omega_I \cap \Omega} c(\mathbf{x}) h_{Im} h_{Jn} d\Omega + \sum_{i,j=1}^d \int_{\Omega_I \cap \Omega} a_{ij}(\mathbf{x}) \frac{\partial h_{Im}}{\partial x_i} \frac{\partial h_{Jn}}{\partial x_j} d\Omega ,$$

$$f_{Im} = \int_{\Omega_I \cap \Omega} f h_{Im} d\Omega ,$$

$$\hat{f}_{Im} = \sum_{i,j=1}^d \int_{\Gamma_I} h_{Im} n_i a_{ij}(\mathbf{x}) \frac{\partial u^{h,p}}{\partial x_j} d\Gamma .$$

In the formulation we distinguish between “interior spheres” and “boundary spheres”. An interior sphere has zero intercept with the boundary, i.e.,  $\Omega_I \cap \Omega = \Omega_I$  (see Fig. 3a). A boundary sphere has a nonzero intercept with the boundary (see Fig. 3b, c). For an interior sphere, therefore,  $\hat{f}_{Im} = 0$  due to compact support and Eq. (6) reduces to:

$$\sum_{J=1}^N \sum_{n \in \mathcal{J}} K_{ImJn} \alpha_{Jn} = f_{Im} .$$

#### 4

##### Imposition of boundary conditions

In this section we discuss how the boundary conditions, given by Eqs. (4) and (5), can be incorporated efficiently.

##### 4.1

###### Natural boundary conditions

In the finite element/finite volume method, due to the Kronecker delta property of the shape functions, only the nodes on the boundary are subjected to the applied boundary conditions. But in the MFS, the basis functions, defined on the spheres, do not satisfy the Kronecker delta condition and hence, any sphere, with nonzero intercept with the boundary contributes to the boundary integral.

Let  $\Gamma_{fI}$  be the intercept of the sphere  $I$  with the boundary  $\Gamma_f$ , see figure 3b, then  $\Gamma_f = \cup_{I \in \mathcal{N}_f} \Gamma_{fI}$ , where  $\mathcal{N}_f$  is the index set of nodes considered. For such a sphere, Eq. (6) applies with

$$\hat{f}_{Im} = \int_{\Gamma_{fI}} h_{Im} f^s d\Gamma .$$

##### 4.2

###### Essential boundary conditions

The imposition of the essential boundary conditions is more difficult in the absence of the Kronecker delta property than the imposition of the natural boundary conditions. In the following we present a technique for the incorporation of the essential boundary conditions and show that a specific arrangement of nodes on the boundary may emulate Kronecker-delta-like properties.

Referring to Fig. 3c we note that any node with nonzero intercept of its sphere with the boundary  $\Gamma_u$  contributes to the boundary integral in Eq. (6). Let  $\Gamma_{uI}$  be the intercept of the sphere  $I$  with the boundary  $\Gamma_u$ , then  $\Gamma_u = \cup_{I \in \mathcal{N}_u} \Gamma_{uI}$ , where  $\mathcal{N}_u$  is the index set of nodes considered. Making use of the chain rule of differentiation, we may now write  $\hat{f}_{Im}$  as

$$\hat{f}_{Im} = \sum_{J=1}^N \sum_{n \in \mathcal{J}} K U_{ImJn} \alpha_{Jn} - f U_{Im} ;$$

where

$$K U_{ImJn} = \sum_{i,j=1}^d \int_{\Gamma_{uI}} \frac{\partial}{\partial x_j} (a_{ij}(\mathbf{x}) h_{Im} h_{Jn} n_i) d\Gamma ,$$

$$f U_{Im} = \sum_{i,j=1}^d \int_{\Gamma_{uI}} u^s \frac{\partial}{\partial x_j} (a_{ij}(\mathbf{x}) n_i h_{Im}) d\Gamma .$$

We note that  $K U_{ImJn}$  is a symmetric stiffness term ( $K U_{ImJn} = K U_{JnIm}$ ) and  $f U_{Im}$  is a (known) forcing term. Hence, Eq. (6) becomes

$$\sum_{J=1}^N \sum_{n \in \mathcal{J}} (K_{ImJn} - K U_{ImJn}) \alpha_{Jn} = f_{Im} - f U_{Im} . \quad (7)$$

This procedure for imposing the Dirichlet boundary conditions is quite general but may be somewhat difficult to implement. Namely, if the nodes are distributed on and near the boundary at random and the boundary is a

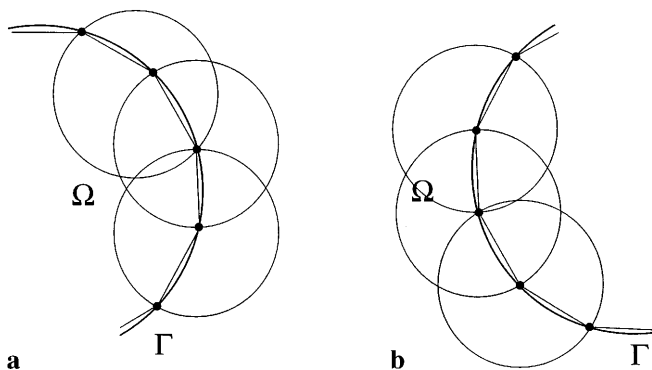


Fig. 4a, b. Nodal arrangement for easy incorporation of Dirichlet boundary conditions on (a) convex and (b) concave boundaries

complex (d-1) dimensional surface, then the computation of the intercepts of the spheres with the boundary surface may become computationally intensive.

To circumvent this difficulty, we propose the special distribution of the boundary spheres shown in Fig. 4. In this construction, we assume that the nodes are placed on the boundary such that the distance between two successive nodes is the radius of the spheres and that there are no nodes whose spheres intercept the boundary other than those that are on the boundary. This nodal arrangement overcomes the problem of finding the intercept of the boundary spheres with complex boundaries. The arrangement also gives rise to a Kronecker delta-like property. Then at any such boundary node  $I$ , the basis functions  $h_{Im}$  are such that

$$h_{I0}(\mathbf{x}_I) = \varphi_I^0(\mathbf{x}_I)$$

and

$$h_{Im}(\mathbf{x}_I) = 0, \quad m \neq 0.$$

From Eq. (1), by construction,

$$\varphi_I^0(\mathbf{x}_I) = \frac{W_I}{\sum_{J=1}^N W_J} = 1.$$

Hence, the basis function  $h_{I0}$  at node  $I$  enjoys the Kronecker delta property

$$h_{I0} = \begin{cases} 1 & \text{at node } I \\ 0 & \text{at all other nodes} \end{cases}$$

whereas the higher-order basis functions exhibit the property

$$h_{Im} = \begin{cases} 0 & \text{at node } I \\ 0 & \text{at all other nodes} \end{cases} \quad \text{for } m \neq 0.$$

Hence

$$v^{h,p}(\mathbf{x} = \mathbf{x}_I) = \alpha_{I0}.$$

Thus the specified value of the field variable  $u$  at node  $I$  on the Dirichlet boundary is taken up by the coefficient of  $h_{I0}$ . The implications are that for specified homogeneous (zero) Dirichlet conditions, we simply remove, from the stiffness matrix, all the rows and columns corresponding to the Shepard functions associated with the nodes that are on the Dirichlet boundary and solve the resulting set of reduced Eq. (7). If inhomogeneous Dirichlet conditions

are specified, we also remove the rows and columns corresponding to the Shepard functions associated with the nodes on the Dirichlet boundary but need to bring the effect of the nonzero prescribed displacements to the right hand side of the governing equations. Hence, Eq. (7) becomes ( $m \neq 0$  with  $I \in \mathcal{N}_u$ )

$$\sum_{J=1}^N \sum_{\substack{n \in \mathcal{J} \\ \text{if } J \in \mathcal{N}_u \\ n \neq 0}} (K_{ImJn} - KU_{ImJn}) \alpha_{Jn} = f_{Im} - fU_{Im} - \bar{f}U_{Im}$$

where

$$\bar{f}U_{Im} = \sum_{J \in \mathcal{N}_u} (K_{ImJ0} - KU_{ImJ0}) u^s(\mathbf{x}_J)$$

and  $\mathbf{x}_J$  is the coordinate of node  $J$ . Of course  $\bar{f}U_{Im} = 0$  when zero Dirichlet conditions are prescribed.

## 5

### Doubly-connected domains: the $n$ -dimensional spherical shell

So far we have concentrated on nodes whose integration domains are singly-connected and therefore coincide with the support. There are certain situations, however, for example, a hole in a plate, or a spherical cavity inside a three-dimensional continuum, when it would be effective to be able to directly model doubly-connected domains. The error introduced in modeling the boundaries of these cavities by placing nodes along their periphery is then eliminated and hence less nodes are required to model such geometries. Also, the known behavior of the solution of the governing equations can be included in the local bases of these nodes and thus higher convergence rates can be attained. To be able to model doubly-connected domains, we decouple the regions of support and integration.

Assume that there is a spherical cavity of radius  $r_i$  and center  $\mathbf{x}_I$  inside the domain  $\Omega$  (see Fig. 5a). We place a node,  $I$ , at the center of the cavity and associate with it a weight function  $W_I$  such that  $\text{supp}(W_I) = B(\mathbf{x}_I, r_i)$ , but we choose the integration domain for this node as

$$\Omega_I \equiv B(\mathbf{x}_I, r_o) \setminus B(\mathbf{x}_I, r_i)$$

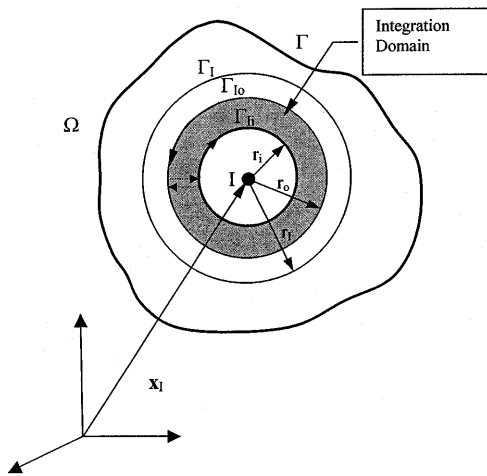
for some  $r_i < r_o \leq r_I$ . We see that Eq. (6) applies with the integral in  $\hat{f}_{Im}$  written as the sum of two integrals (applying contour integration as shown in Fig. 5a)

$$\begin{aligned} \hat{f}_{Im} = & \sum_{i,j=1}^d \oint_{\Gamma_{I_o}} a_{ij}(\mathbf{x}) h_{Im} n_i \frac{\partial u^{h,p}}{\partial x_j} d\Gamma \\ & + \sum_{i,j=1}^d \oint_{\Gamma_{I_i}} a_{ij}(\mathbf{x}) h_{Im} n_i \frac{\partial u^{h,p}}{\partial x_j} d\Gamma, \end{aligned} \quad (8)$$

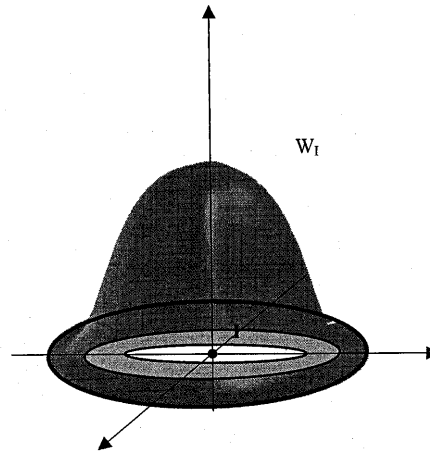
where  $\Gamma_{I_o} = S(\mathbf{x}_I, r_o)$  and  $\Gamma_{I_i} = S(\mathbf{x}_I, r_i)$ . We consider two cases:

**Case (1)  $r_o = r_I$ :** The first integral in Eq. (8) is zero due to the property of compact support and we have

$$\hat{f}_{Im} = \sum_{i,j=1}^d \oint_{\Gamma_{I_i}} a_{ij}(\mathbf{x}) h_{Im} n_i \frac{\partial u^{h,p}}{\partial x_j} d\Gamma.$$



**a** A domain with a spherical cavity modeled using spherical shells



**b** The weight function  $W_I$  at node I

**Fig. 5a, b.** A domain  $\Omega$  with a spherical cavity of radius  $r_i$  is shown. Node I is placed at the center of the cavity. The weight function,  $W_I$ , at node I has a support radius of  $r_i$ . The integration domain associated with the node I is a spherical shell of inner radius  $r_i$  and outer radius  $r_o$ .

Usually we have some boundary data prescribed on the inside surface of the cavity which can be incorporated using the techniques described in the previous section.

**Case (2)  $r_o < r_i$ :** In this case we have to use Eq. (8) in its full form.

## 6 Numerical integration

Numerical integration is an important ingredient of a meshless method. In the finite element method the functions to be integrated are usually polynomials (or mapped polynomials) whereas in the MFS, the PU shape functions are rational (nonpolynomial) functions. In the finite element method, the elements can be mapped to  $n$ -dimensional cubes and hence Gauss-Legendre product rules are probably most appropriate (Stroud, 1971). Since in the MFS, the integration domains are spheres or spherical shells for interior domains and general sectors for boundary spheres, a separate class of integration rules is required. In Appendix A we state, without proof, Gaussian product rules of cubature on two-dimensional sectors and annuli. Even though cubature rules exist for circular annuli as well as spheres and hyperspheres (Peirce, 1957a, b; Lether, 1971; Stroud, 1971; Stoyanova, 1997), rules for annular sectors seem not to have been published. Note that the integration rules we are using are different from those in Atluri et al. (1999a).

**Interior disk** For an interior disk (see Fig. 6a, b), we use Corollary A.1 and are able to integrate with any given precision. The integration points are on equally spaced radii and the integration weights are independent of angular position (Gauss-Chebyshev rule in the  $\theta$ -direction). For the two-dimensional solutions considered in Sect. 7, a rather large number of integration points are used per disk (6 integration points along each of 24 radial directions).

**Boundary disk** We categorize the boundary sectors into two major groups depending on the angle  $\phi_0$  that the radii joining the center of the disk to the two intercepts of the disk on  $\Gamma$  make interior to the domain:

**Type I sector:  $\phi_0 \leq \pi$  (see Fig. 7)** In Appendix A we state the rule that allows us to perform numerical cubature on this sector to any desired order of accuracy. But roots of higher-order orthogonal polynomials for every boundary

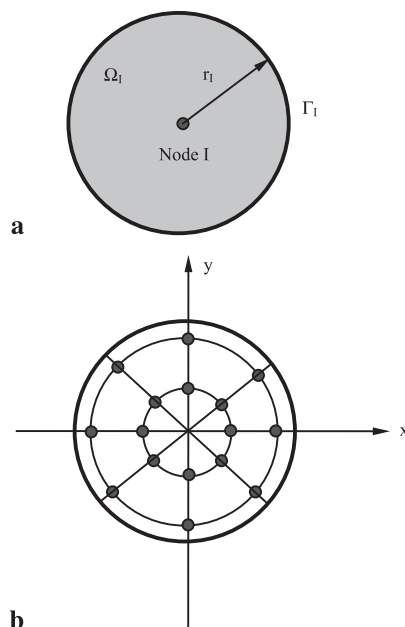


**Fig. 6a, b.** An interior disk is shown in (a). In (b) we display the integration points (schematically) corresponding to an accuracy of order  $k=7$ . Note that the integration points are on equally spaced radii and the integration weights are independent of angular position

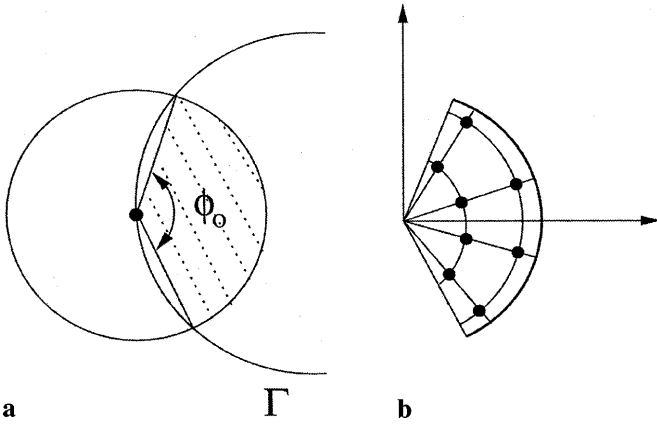


Fig. 7a, b. Type I boundary sector (a) and the distribution of integration points (b)

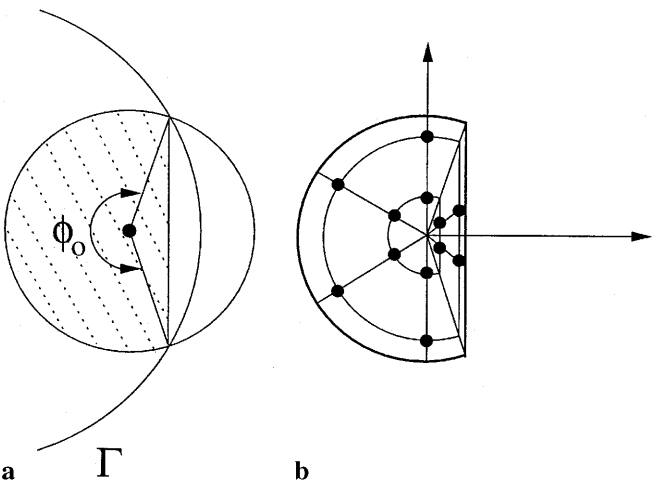


Fig. 8a, b. Type II boundary sector (a) and the distribution of integration points (b)

sector need be evaluated. To circumvent this expense, we propose an “engineering solution” and use Gauss-Legendre quadrature in the  $\theta$ -direction.

**Type II sector :**  $\phi_0 > \pi$  (see Fig. 8) This type of boundary sector is more expensive to handle. We decompose a Type II sector into a sector for which the rules of the Type I sector can be used and a triangle as shown in Fig. 8b. For the triangle we use a product rule based on Gauss-Legendre quadrature.

**7 Numerical examples**

In this section we present numerical examples in one and two dimensions demonstrating the above formulation. A simple problem involving a bar with distributed loading is solved in one-dimension, followed by a one-dimensional high Peclet number flow problem. In two-dimensions we first solve a Poisson problem with mixed boundary conditions and then two linear elasticity problems. Corresponding to each distinct type of equation solved by the MFS, a patch test was performed and the method passed the patch test in each case.

**7.1 The MFS in  $R^1$ : a bar with distributed loading**

**7.1.1 Formulation**

In  $R^1$  the “spheres” reduce to line-segments (as shown in Fig. 9a). We solve the following problem of a bar of unit length, subjected to a distributed loading:

$$\frac{d^2 u(x)}{dx^2} + f(x) = 0 \quad \text{in } \Omega = (0, 1)$$

$$u = u^s \quad \text{at } x = 0$$

$$\frac{du}{dx} = f^s \quad \text{at } x = 1$$

The parameters  $u^s$  and  $f^s$  and the function  $f(x)$  are chosen so that the analytical solution  $u$  is given by the following expression:

$$u(x) = \frac{1}{2} \left( x - \frac{x^3}{3} \right) + 2x + 1 .$$

The weight function defined in Sect. 2.1 is used to generate the Shepard partition of unity. At each node  $I$ , the following shape functions were used;

$$\{ \varphi_I^0(x), \varphi_I^0(x)(x - x_I)/r_I \}$$

to attain linear consistency. Figure 9a shows a plot of these shape functions for a typical node within the domain. The discretized equation corresponding to the  $I$ th node and  $m$ th degree of freedom is given by Eq. (6) where the integrals are

$$K_{ImJn} = \int_{x_1}^{x_2} \frac{dh_{Im}}{dx} \frac{dh_{Jn}}{dx} dx$$

$$f_{Im} = \int_{x_1}^{x_2} f(x) h_{Im} dx$$

$$\hat{f}_{Im} = \begin{cases} 0 & \text{for an “interior sphere”} \\ f^s h_{Im}(x=1) & \text{for a sphere on the Neumann boundary} \\ \sum_{j=1}^N \sum_{n \in \mathcal{J}} KU_{ImJn} \alpha_{Jn} - fU_{Im} & \text{for a sphere on the Dirichlet boundary} \end{cases}$$

where

$$KU_{ImJn} = - \left[ \frac{d}{dx} (h_{Im} h_{Jn}) \right]_{x=0}$$

$$fU_{Im} = -u^s \left[ \frac{dh_{Im}}{dx} \right]_{x=0}$$

it being understood that  $x_1 = \max(0, x_I - r_I)$  and  $x_2 = \min(1, x_I + r_I)$ .

**7.1.2 Numerical results**

Both regular and arbitrary distributions of nodes have been used to solve the problem. Figure 9b shows the result

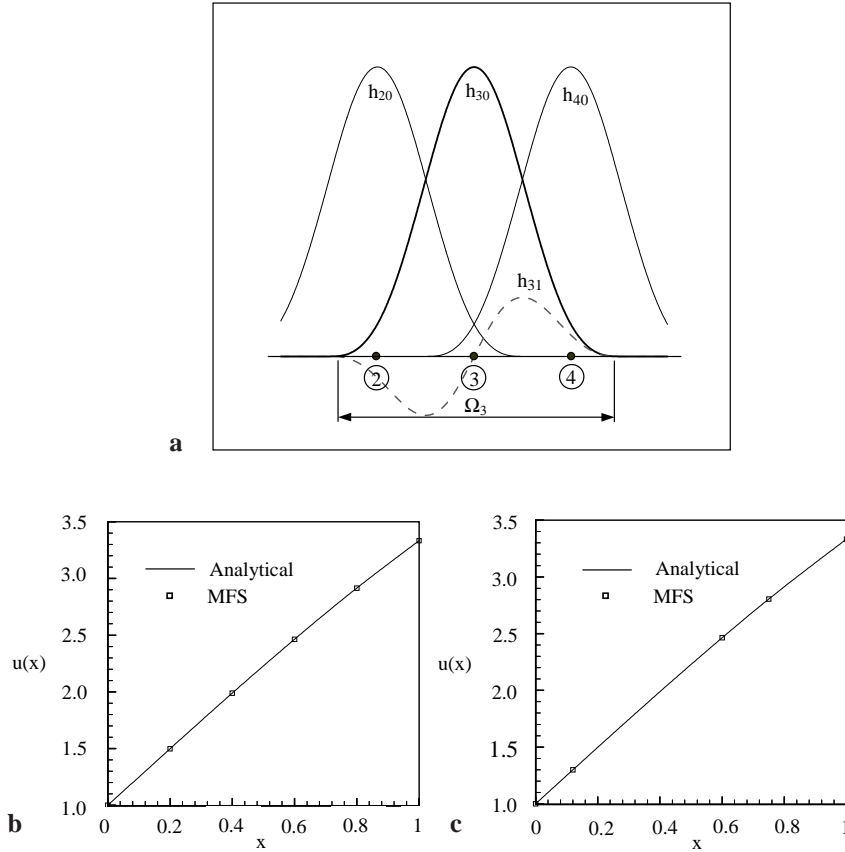


**Fig. 9a-c.** A bar of unit length with distributed loading. In (a) a part of the bar is shown with 3 nodes. The Shepard functions  $h_{i0}$  ( $i= 2,3,4$ ) are plotted at each node. At node 3, a higher order shape function  $h_{31} = ((x-x_3)/r_3)h_{30}$  is also plotted. The sphere at each node  $I$  ( $\Omega_I$ ) reduces to a line segment in one-dimension. In (b) and (c) the displacement field  $u(x)$  is plotted as a function of the distance along the bar corresponding to the boundary conditions and loading given in section 7.1.1. The numerical result in (b) corresponds to a regular distribution of 6 nodes on the bar while that in (c) corresponds to an arbitrary distribution of 5 nodes

when six nodes are distributed regularly. Figure 9c shows the solution when the same problem is solved using five nodes with arbitrary distances between them.

**7.2 The MFS in  $R^1$ : a high Peclet number flow problem**

**7.2.1 Formulation**

We consider the following problem of steady state heat conduction in one dimension with prescribed velocity  $v$  as discussed in Bathe (1996). The temperature is prescribed at two points,  $x = 0$  and  $x = L$  and we intend to compute the temperature in  $(0, L)$ . The governing differential equation for the temperature,  $\theta$ , is

$$\frac{d^2\theta}{dx^2} = \frac{Pe}{L} \frac{d\theta}{dx} \quad \text{in } (0, L)$$

with the boundary conditions;

$$\theta = \theta_L \quad \text{at } x = 0$$

$$\theta = \theta_R \quad \text{at } x = L$$

where the Peclet number is defined as  $Pe = (vL)/\alpha$  ( $\alpha$  is the thermal diffusivity of the fluid). The exact solution to this problem is given by

$$\frac{\theta - \theta_L}{\theta_R - \theta_L} = \frac{\exp\left(\frac{Pe}{L}x\right) - 1}{\exp(Pe) - 1}$$

With increase in the Peclet number, the solution curve shows a strong boundary layer at  $x = L$ . The solution using a simple Galerkin finite element scheme leads to severe numerical difficulties and a variety of upwind-type procedures have been proposed to solve the problem (see Bathe, 1996). In this work we apply the MFS and simply use as our local approximation spaces

$$V_I^{h,p} = \text{span}\{1, \exp(Pe x/L)\} .$$

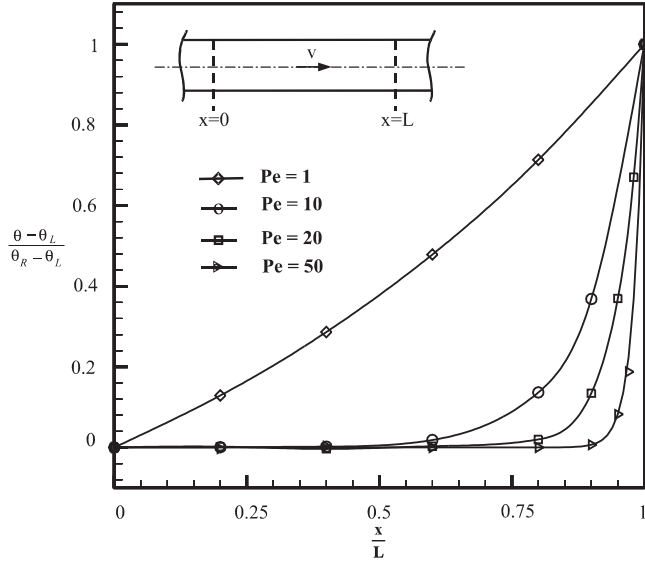
**7.2.2 Numerical results**

Figure 10 shows the numerical solutions obtained using the MFS, with quite arbitrarily spaced nodes, plotted on the analytical solution curves for  $Pe = 1, 10, 20$  and  $50$ . Due to the solution space chosen we expect a very accurate response with no “wiggles”, and this is the case, see Fig. 10. It seems that the method of finite spheres has significant potential for the development of fluid mechanics solution schemes to solve two- and three-dimensional flow problems.

**7.3 The MFS in  $R^2$ : the Poisson equation on the bi-unit square**

**7.3.1 Formulation**

We consider a problem in a single field variable defined on  $R^2$ . We seek a function  $u(x, y)$  satisfying the Poisson equation



**Fig. 10.** Results of the high Peclet number flow problem. The normalized temperature distribution is plotted against normalized distance along the flow direction for four different Peclet numbers ( $Pe = 1, 10, 20$  and  $50$ ). Continuous lines correspond to the analytical solution. The solution obtained using the method of finite spheres is plotted corresponding to arbitrary distributions of nodes along the domain

$$\frac{\partial^2 u}{\partial x^2} + \frac{\partial^2 u}{\partial y^2} + f(x, y) = 0 \quad \text{in } \Omega = (-1, 1) \times (-1, 1)$$

subject to the boundary conditions (see Fig. 11)

$$u = u^s(x, y) \quad \text{on } \Gamma_a$$

$$\frac{\partial u}{\partial y} = 0 \quad \text{on } \Gamma_b$$

$$\frac{\partial u}{\partial x} = -f^s(x, y) \quad \text{on } \Gamma_c$$

$$\frac{\partial u}{\partial y} = 0 \quad \text{on } \Gamma_d$$

The functions  $f(x, y)$ ,  $f^s(x, y)$  and  $u^s(x, y)$  are chosen such that the analytical solution  $u(x, y)$  is

$$u(x, y) = (7x + x^7) \cos(\pi y)$$

The discretized equation corresponding to the  $m$ th degree of freedom of the  $I$ th node is given by Eq. (6) where the integrals are

$$K_{ImJn} = \int_{\Omega_I \cap \Omega} \left( \frac{\partial h_{Im}}{\partial x} \frac{\partial h_{Jn}}{\partial x} + \frac{\partial h_{Im}}{\partial y} \frac{\partial h_{Jn}}{\partial y} \right) d\Omega$$

$$f_{Im} = \int_{\Omega_I \cap \Omega} f(x, y) h_{Im} d\Omega$$

$$\hat{f}_{Im} = \begin{cases} 0 & \text{for an "interior sphere"} \\ 0 & \text{for spheres on } \Gamma_b \text{ and } \Gamma_d \\ \int_{\Gamma_{c_I}} f^s h_{Im} d\Omega & \text{for a sphere on } \Gamma_c \\ \sum_{j=1}^N \sum_{n \in \mathcal{J}} K_{ImJn} \alpha_{Jn} - f_{Im} & \text{for a sphere on } \Gamma_a \end{cases}$$

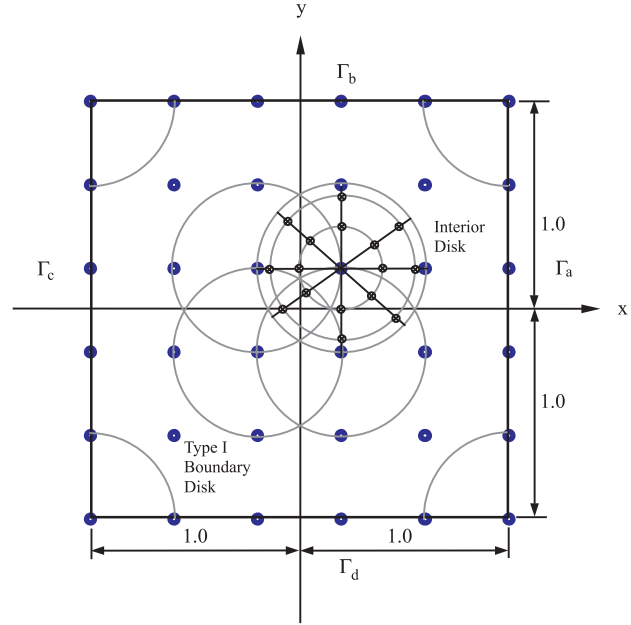


**Fig. 11.** A regular arrangement of 36 nodes is shown on the domain on which the Poisson problem is defined. Some of the interior disks as well as some type I boundary disks are also plotted. Some selected integration points are shown for one of the interior disks as crosshatched circles  $\otimes$  (the actual number of integration points used in this example was 144 per interior disk)

where

$$KU_{ImJn} = \int_{\Gamma_{a_I}} \frac{\partial}{\partial x} (h_{Im} h_{Jn}) d\Gamma$$

$$fU_{Im} = \int_{\Gamma_{a_I}} u^s \frac{\partial h_{Im}}{\partial x} d\Gamma$$

and  $\Gamma_a = \cup_{I \in \mathcal{N}_a} \Gamma_{a_I}$  and  $\Gamma_c = \cup_{I \in \mathcal{N}_c} \Gamma_{c_I}$ ,  $\mathcal{N}_a$  and  $\mathcal{N}_c$  being the index set of nodes whose spheres have nonzero intercepts with the boundaries  $\Gamma_a$  and  $\Gamma_c$  respectively.

### 7.3.2

#### Numerical results

Figure 11 shows the discretization of the domain using a regular arrangement of 36 nodes. In Fig. 12 we present the MFS shape functions at an interior node. The nonpolynomial nature of the shape functions is quite evident. In Fig. 13a we present the MFS solution  $u(x)$  superposed on the analytical one along two lines  $y = 0$  and  $y = 1$ . In Fig. 13b the solution  $u(y)$  (as computed by the MFS) is shown as a function of the spatial coordinate  $y$  along the boundary  $\Gamma_a$  (i.e.  $x = 1$ ) together with the analytical solution. Note that the essential boundary condition prescribed along this boundary is exactly satisfied at the nodes but only approximately (in a weak sense) in-between the nodes.

### 7.4

#### Linear elasticity problems in $R^2$

##### 7.4.1

#### Formulation

In this section we derive the weak form and the discretized equations for a linear elastic continuum in 2D. The system

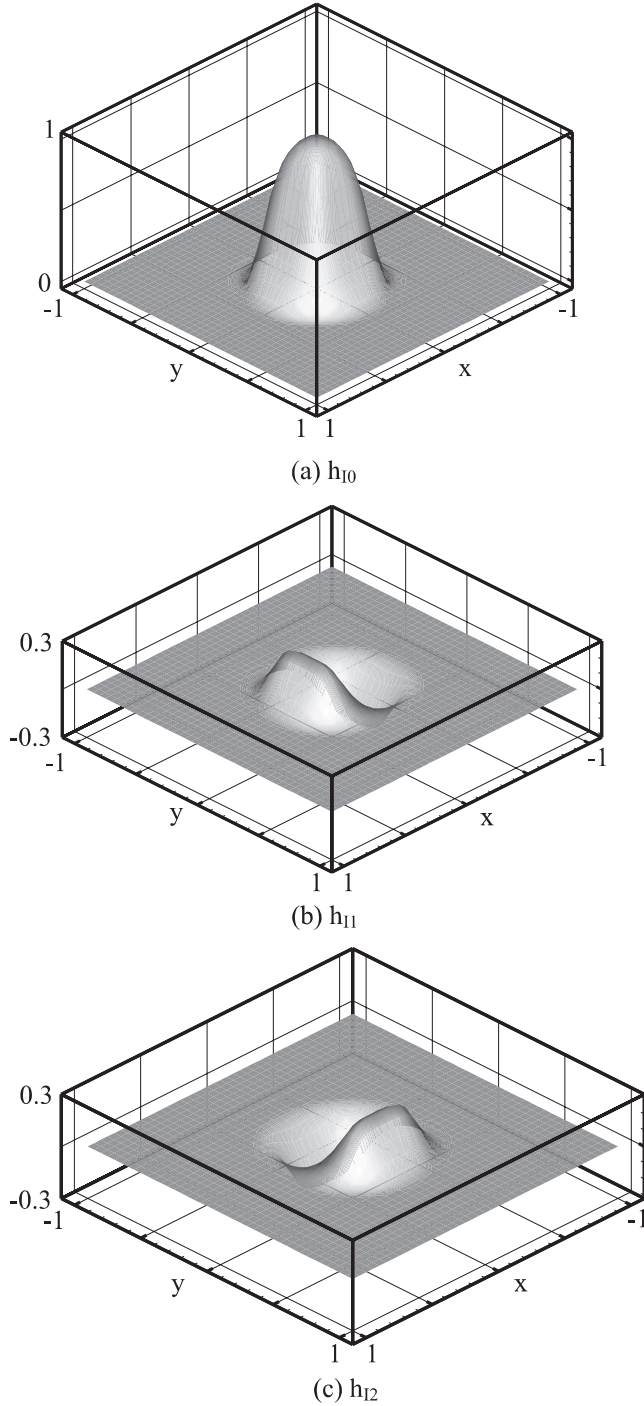


Fig. 12a-c. Three shape functions ( $h_{10}$ ,  $h_{11}$  and  $h_{12}$ ) at an interior node are shown.  $h_{10}$  is the Shepard function at the node, while  $h_{11} = ((x-x_1)/r_1) h_{10}$  and  $h_{12} = ((y-y_1)/r_1) h_{10}$

of governing differential equations and the boundary conditions can be written as:

Equilibrium equations:

$$\partial_{\epsilon}^T \boldsymbol{\tau} + \mathbf{f}^B = \mathbf{0} \quad \text{in } \Omega \quad (9)$$

Strain-displacement relationships:

$$\boldsymbol{\epsilon} = \partial_{\epsilon} \mathbf{u} \quad \text{in } \Omega \quad (10)$$

Linear elastic constitutive relationship:

$$\boldsymbol{\tau} = \mathbf{C} \boldsymbol{\epsilon} \quad \text{in } \Omega \quad (11)$$

Boundary conditions:

$$\mathbf{N} \boldsymbol{\tau} = \mathbf{f}^s \quad \text{on } \Gamma_f \quad (12)$$

$$\mathbf{u} = \mathbf{u}^s \quad \text{on } \Gamma_u \quad (13)$$

In the Eqs. (9) to (13),  $\mathbf{u}$ ,  $\boldsymbol{\epsilon}$  and  $\boldsymbol{\tau}$  are the displacement, stress and strain vectors,  $\mathbf{C}$  is the elasticity matrix,  $\mathbf{f}^s$  is the prescribed traction vector on the Neumann boundary  $\Gamma_f$ ,  $\mathbf{u}^s$  is the vector of prescribed displacements on the Dirichlet boundary  $\Gamma_u$  (note that the domain boundary  $\Gamma = \Gamma_f \cup \Gamma_u$ ),  $\mathbf{f}^B$  is the body force vector (including inertia terms),  $\partial_{\epsilon}$  is a linear gradient operator and  $\mathbf{N}$  is the matrix of direction cosine components of a unit normal to the domain boundary (positive outwards). In  $R^2$  these vectors and matrices are written as:

$$\mathbf{u} = [u(x, y) \quad v(x, y)]^T \quad (14)$$

$$\boldsymbol{\epsilon} = [\epsilon_{xx} \quad \epsilon_{yy} \quad \gamma_{xy}]^T \quad (15)$$

$$\boldsymbol{\tau} = [\tau_{xx} \quad \tau_{yy} \quad \tau_{xy}]^T \quad (16)$$

$$\mathbf{f}^s = [f_x^s(x, y) \quad f_y^s(x, y)]^T$$

$$\mathbf{u}^s = [u^s(x, y) \quad v^s(x, y)]^T$$

$$\partial_{\epsilon} = \begin{bmatrix} \partial/\partial x & 0 \\ 0 & \partial/\partial y \\ \partial/\partial y & \partial/\partial x \end{bmatrix} \quad (17)$$

$$\mathbf{N} = \begin{bmatrix} n_x & 0 & n_y \\ 0 & n_y & n_x \end{bmatrix} \quad (18)$$

$$\mathbf{C} = \begin{bmatrix} c_{11} & c_{12} & 0 \\ c_{12} & c_{11} & 0 \\ 0 & 0 & c_{33} \end{bmatrix}$$

where

$$c_{11} = \frac{E}{1 - \nu^2}, \quad c_{12} = \frac{E\nu}{1 - \nu^2} \quad \text{and} \quad c_{33} = \frac{E}{2(1 + \nu)}$$

for plane stress conditions

$$c_{11} = \frac{E(1 - \nu)}{(1 + \nu)(1 - 2\nu)}, \quad c_{12} = \frac{E\nu}{(1 + \nu)(1 - 2\nu)} \quad \text{and}$$

$$c_{33} = \frac{E}{2(1 + \nu)} \quad \text{for plane strain conditions}$$

$E$  and  $\nu$  being the Young's modulus and Poisson's ratio of the material, respectively.

We have the following approximation for the displacement field

$$\mathbf{u}(x, y) \simeq \sum_{J=1}^N \sum_{n \in \mathcal{I}} \mathbf{H}_{Jn}(x, y) \alpha_{Jn} = \mathbf{H}(x, y) \mathbf{U}, \quad (19)$$

where

$$\mathbf{U} = [\alpha_{10} \quad \alpha_{11} \quad \alpha_{12} \quad \cdots \quad \alpha_{Jn} \quad \cdots]^T$$

is the vector of nodal unknowns (not nodal displacements unless the Kronecker delta property is satisfied by the shape functions), and

$$\alpha_{Jn} = [u^{Jn} \quad v^{Jn}]$$

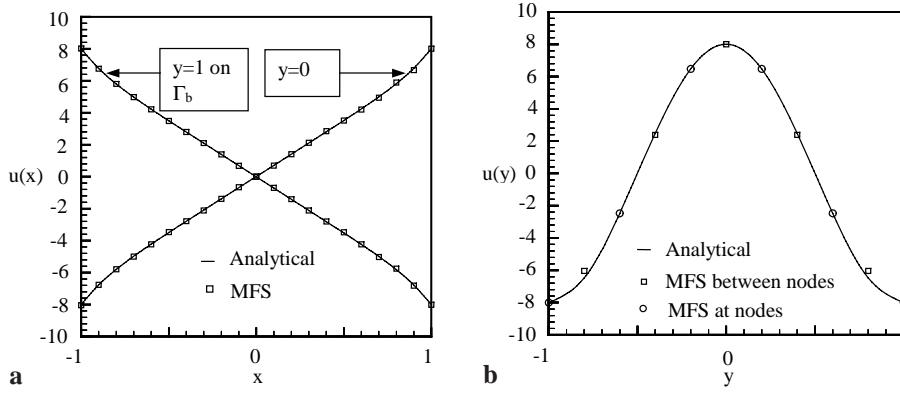


**Fig. 13a, b.** Results of the Poisson problem. In (a) the field variable  $u(x)$  is plotted as a function of  $x$  for two values of  $y$  ( $= 0, 1$ ). In (b) the Dirichlet boundary  $\Gamma_a$  is considered. The MFS solution is plotted as a function of  $y$  with the analytical solution

is the vector of nodal unknowns at node  $J$  corresponding to the  $n$ th degree of freedom ( $u^{Jn}$  and  $v^{Jn}$  are the nodal variables for the  $x$  and  $y$  direction displacements at node  $J$  corresponding to the  $n$ th degree of freedom). The nodal shape function matrix corresponding to the  $n$ th degree of freedom is

$$\mathbf{H}_{Jn}(x, y) = \begin{bmatrix} h_{Jn}(x, y) & 0 \\ 0 & h_{Jn}(x, y) \end{bmatrix}. \quad (20)$$

Hence, the discretized versions of Eqs. (10) and (11) are

$$\boldsymbol{\epsilon}(x, y) \simeq \sum_{J=1}^N \sum_{n \in \mathcal{J}} \mathbf{B}_{Jn}(x, y) \boldsymbol{\alpha}_{Jn} = \mathbf{B}(x, y) \mathbf{U} \quad (21)$$

and

$$\boldsymbol{\tau}(x, y) \simeq \sum_{J=1}^N \sum_{n \in \mathcal{J}} \mathbf{C} \mathbf{B}_{Jn}(x, y) \boldsymbol{\alpha}_{Jn} = \mathbf{C} \mathbf{B}(x, y) \mathbf{U}, \quad (22)$$

where the strain–displacement matrix  $\mathbf{B}(x, y)$  in Eq. (21) is partitioned as

$$\mathbf{B}(x, y) = [\mathbf{B}_{10}(x, y) \ \mathbf{B}_{11}(x, y) \ \cdots \ \mathbf{B}_{Jn}(x, y) \ \cdots]$$

where

$$\mathbf{B}_{Jn}(x, y) = \partial_{\epsilon} \mathbf{H}_{Jn}(x, y) = \begin{bmatrix} \partial h_{Jn}/\partial x & 0 \\ 0 & \partial h_{Jn}/\partial y \\ \partial h_{Jn}/\partial y & \partial h_{Jn}/\partial x \end{bmatrix}. \quad (23)$$

At each node  $I$ , we may write the Bubnov–Galerkin weak form corresponding to the  $m$ th degree of freedom as (from Eq. (9))

$$\int_{\Omega_f \cap \Omega} \mathbf{H}_{Im} \partial_{\epsilon}^T \boldsymbol{\tau} \, d\Omega + \int_{\Omega_f \cap \Omega} \mathbf{H}_{Im} \mathbf{f}^B \, d\Omega = \mathbf{0}. \quad (24)$$

In 2D these are two equations corresponding to the two coordinate directions. Applying Green’s theorem and Eqs. (22) and (23) we obtain the discretized system of algebraic equations

$$\sum_{J=1}^N \sum_{n \in \mathcal{J}} \mathbf{K}_{ImJn} \boldsymbol{\alpha}_{Jn} = \mathbf{f}_{Im} + \hat{\mathbf{f}}_{Im} \quad (25)$$

which is the vector form of Eq. (6). In Eq. (25), the various matrices and vectors are as follows;

$$\mathbf{K}_{ImJn} = \int_{\Omega_f \cap \Omega} \mathbf{B}_{Im}^T \mathbf{C} \mathbf{B}_{Jn} \, d\Omega \quad (26)$$

$$\mathbf{f}_{Im} = \int_{\Omega_f \cap \Omega} \mathbf{H}_{Im} \mathbf{f}^B \, d\Omega \quad (27)$$

$$\hat{\mathbf{f}}_{Im} = \int_{\Gamma_f} \mathbf{H}_{Im} \mathbf{N} \boldsymbol{\tau} \, d\Gamma \quad (28)$$

It is only this last Eq. (28) that is different for the different types of spheres (disks) that we encounter.

If  $I$  is a node associated with an “internal sphere”, then

$$\hat{\mathbf{f}}_{Im} = \mathbf{0}$$

from compact support.

If  $I$  is a node with an annular integration domain (see Sect. 5), with internal boundary  $\Gamma_{Ii}$  and external boundary  $\Gamma_{Io}$ , then

$$\hat{\mathbf{f}}_{Im} = \oint_{\Gamma_{Io}} \mathbf{H}_{Im} \mathbf{N} \boldsymbol{\tau} \, d\Gamma + \oint_{\Gamma_{Ii}} \mathbf{H}_{Im} \mathbf{N} \boldsymbol{\tau} \, d\Gamma. \quad (29)$$

If  $I$  is a node on the Neumann boundary, then from Eq. (12),

$$\hat{\mathbf{f}}_{Im} = \int_{\Gamma_{f_i}} \mathbf{H}_{Im} \mathbf{f}^s \, d\Gamma \quad (30)$$

where  $\Gamma_f = \cup_{I \in \mathcal{N}_f} \Gamma_{f_i}$ ,  $\mathcal{N}_f$  being the index set of nodes with spheres having nonzero intercepts on  $\Gamma_f$ .

If  $I$  is a node on the Dirichlet boundary, then

$$\hat{\mathbf{f}}_{Im} = \sum_{J=1}^N \sum_{n \in \mathcal{J}} \mathbf{K} \mathbf{U}_{ImJn} \boldsymbol{\alpha}_{Jn} - \mathbf{f} \mathbf{U}_{Im} \quad (31)$$

where

$$\mathbf{K} \mathbf{U}_{ImJn} = \int_{\Gamma_{u_i}} \mathbf{H}_{Im} \mathbf{N} \mathbf{C} \mathbf{B}_{Jn} \, d\Gamma + \int_{\Gamma_{u_i}} \mathbf{B}_{Im}^T \mathbf{C} \mathbf{N}^T \mathbf{H}_{Jn} \, d\Gamma \quad (32)$$

and

$$\mathbf{f} \mathbf{U}_{Im} = \int_{\Gamma_{u_i}} \mathbf{B}_{Im}^T \mathbf{C} \mathbf{N}^T \mathbf{u}^s \, d\Gamma \quad (33)$$

where  $\Gamma_u = \cup_{I \in \mathcal{N}_u} \Gamma_{u_i}$ ,  $\mathcal{N}_u$  being the index set of nodes with spheres having nonzero intercepts on  $\Gamma_u$ . Note that the stiffness matrix  $\mathbf{K} \mathbf{U}$  is symmetric.

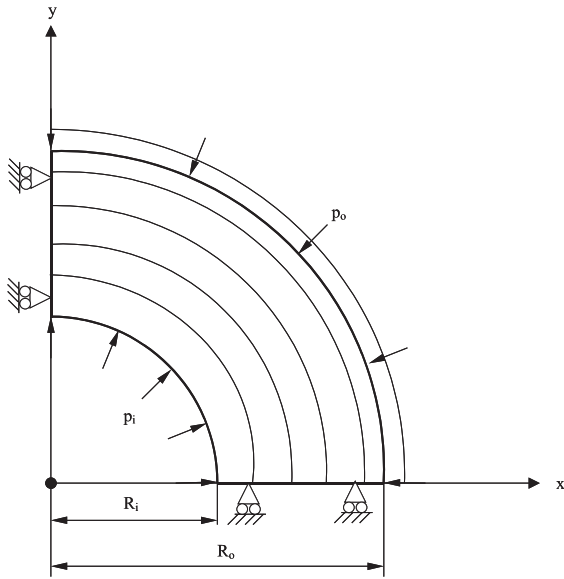


Fig. 14. A quadrant of the thick-walled pressure vessel (in plane stress). All the nodes are placed at the origin of the coordinate system. The integration domain corresponding to each node is an annular sector of inner radius  $R_i$

It is interesting to note that this formulation gives rise to the same system matrices as obtained when the applied displacements are introduced into a variational formulation of the problem via Lagrange multipliers and the Lagrange multipliers are replaced by their “physical significances” as described by Washizu (1975). This formulation has also been adopted by Lu et al. (1994) in their

implementation of essential boundary conditions in the context of the element free Galerkin methods.

Another point to note is that we may incorporate the Dirichlet conditions by the special arrangement of nodes on the boundary as discussed in Sect. 4.2.

Patch tests were performed on a bi-unit square (both in plane stress and in plane strain conditions) using the above formulation and they were passed with as few as four nodes placed at the corners.

#### 7.4.2 Numerical results

**Thick walled pressure vessel in plane stress** We consider a thick-walled pressure vessel of external radius  $R_o (= 10)$  and internal radius  $R_i (= 5)$ , subjected to uniform internal pressure  $p_i$  and external pressure  $p_o$ . The material properties of the cylinder wall are chosen as  $E = 100$  and  $\nu = 0.3$ . As shown in Fig. 14, one quadrant of the cylinder is discretized. The nodes for all the disks are superimposed at the origin. All nodes are associated with annular integration domains, and the integration annuli have the same inner radius ( $R_i$ ) but different outer radii. To be able to incorporate the Neumann boundary conditions at  $R_o$ , some annuli are chosen to have outer radii greater than  $R_o$  (see Fig. 14). Figures 15 and 16 present results of two numerical experiments. In the first one (Fig. 15)  $p_o = p_i = 1.0$ . In the second experiment (Fig. 16)  $p_i = 10$  and  $p_o = 0$ . The computed radial displacement field is plotted against the analytical solution in Fig. 16a. Figure 16b shows the radial ( $\sigma_{rr}$ ) and hoop ( $\sigma_{\theta\theta}$ ) stresses normalized with the internal pressure ( $p_i$ ). In this solution 12 nodes were used.

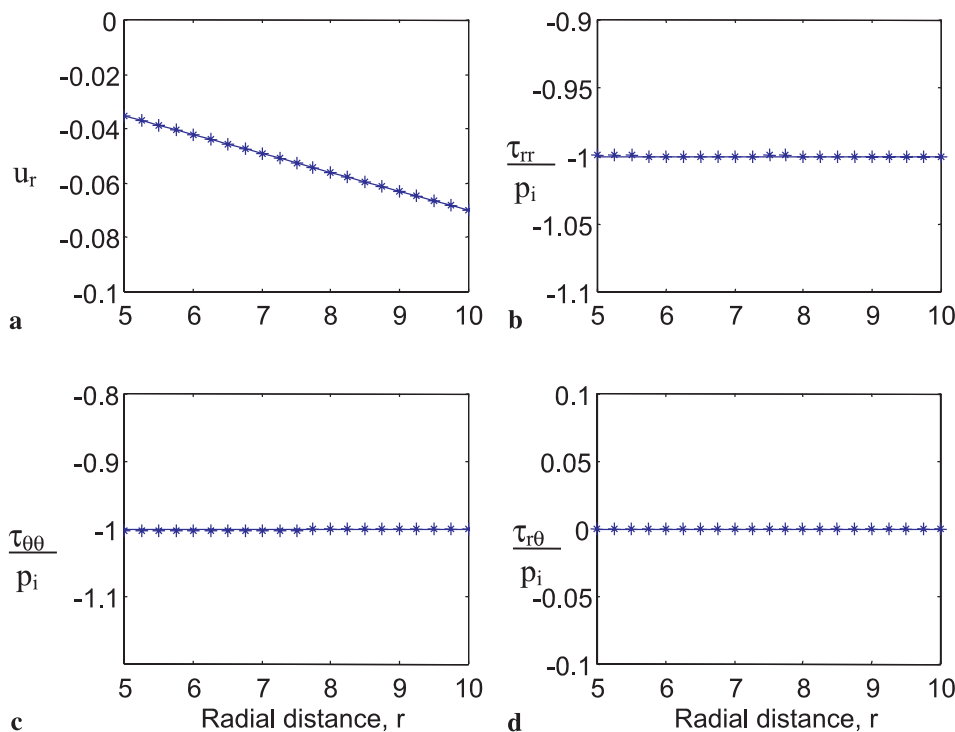
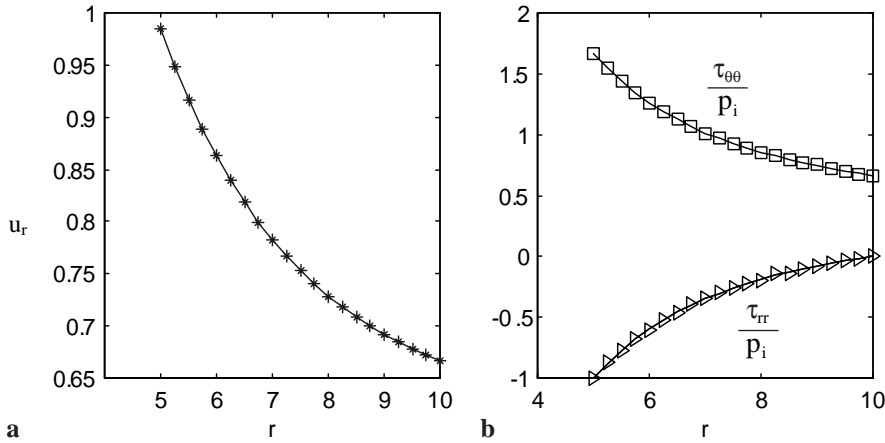


Fig. 15a–d. Results of the pressure vessel problem for  $p_i = p_o = 1.0$ . The radial displacement ( $u_r$ ), the normalized radial stress ( $\tau_{rr}$ ), hoop stress ( $\tau_{\theta\theta}$ ) and shear stress ( $\tau_{r\theta}$ ) are plotted along a radius of the cylinder in (a), (b), (c) and (d) respectively. Continuous lines indicate analytical solution whereas the MFS solution is plotted with asterisks



**Fig. 16.** (a) Radial displacement field  $u_r$  and (b) normalized radial ( $\tau_{rr}$ ) and hoop ( $\tau_{\theta\theta}$ ) stresses in the cylinder wall corresponding to  $p_i=10$  and  $p_0=0$ . Continuous lines indicate analytical solution whereas the MFS solution is indicated by asterisks (\*), triangles ( $\Delta$ ), or squares ( $\square$ )

### A cantilever plate in plane strain with uniformly distributed loading

In this problem we consider a cantilever plate in plane strain conditions as shown in Fig. 17a. The material properties of the plate are chosen as  $E = 100$  and  $\nu = 0.3$ . A uniformly distributed load of magnitude  $w = 1.0$  per unit length is applied as shown. Figure 17b shows the convergence in strain energy when a h-type uniform refinement is performed. In this analysis the local basis of each node has been chosen as a complete polynomial of second degree. The strain energy of the limit

solution of the system is obtained by solving the same problem using a  $50 \times 50$  mesh of 9-noded finite elements. An order of convergence of 4.078 is observed which compares very well with the theoretical value of 4. This measured rate of convergence is much better than the one obtained in the classical finite element analysis when ungraded meshes are used, and might indicate a robustness of the MFS.

### 8 Concluding remarks

The objective of this paper was to present some of our latest developments in meshless methods. We reviewed several existing meshless techniques and concluded that none of the methods is effective for general applications. However, we found the meshless local Petrov–Galerkin (MLPG) method to be conceptually the most attractive. We are therefore using this concept in our research to obtain an effective meshless solution procedure.

In this paper we propose a specialized form of the MLPG approach – the method of finite spheres (MFS) – which appears to have many valuable attributes. The method is truly meshless and the boundary conditions are incorporated relatively easily, in particular when a special arrangement of nodes on the boundary is used. Moreover, a new technique for modeling doubly-connected domains is presented in this paper using the concept of  $n$ -dimensional spherical shells as integration domains. The solutions of various example problems are given to demonstrate the MFS.

An important feature of the method is the numerical integration scheme used. We employ Gaussian product rules for integration on two-dimensional annuli and annular sectors. A generalization would be used in three dimensions. The number of integration points employed is, however, rather large compared to those used in the conventional finite element method. This is attributed to the fact that in the conventional finite element method the functions to be integrated are polynomials (or mapped polynomials) but in the MFS complicated rational (non-polynomial) functions have to be integrated.

Considerable improvements in the choice of functions and the numerical integration schemes must be achieved before the method would become, in efficiency, competitive with the existing finite element procedures. Such

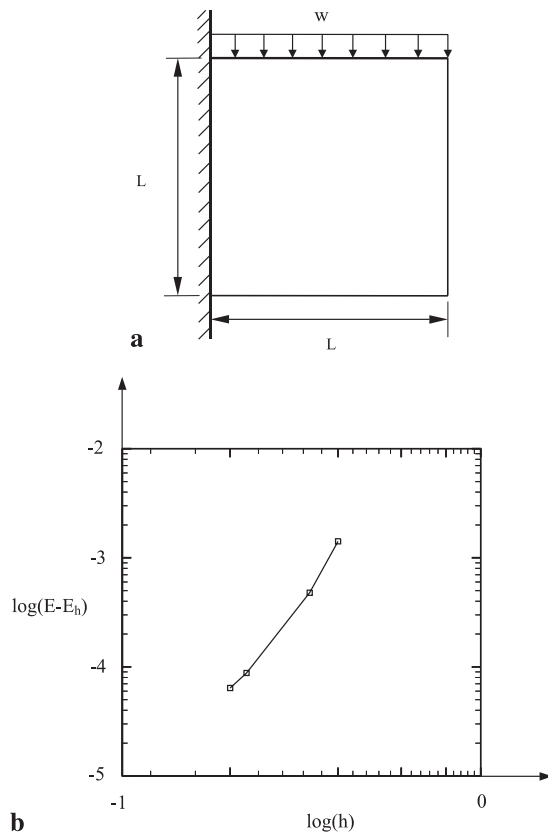


**Fig. 17.** (a) Cantilever plate ( $L=2.0$ ) in plane strain. Uniformly distributed load of magnitude  $w=1.0$  per unit length is applied.  $E=100$ ,  $\nu=0.3$ . In (b) the convergence of the strain energy ( $E_h$ ) with decrease in radius of support ( $h$ ) is shown. The strain energy of the limit solution,  $E$ , is obtained by solving the same problem using a  $50 \times 50$  mesh of 9-noded finite elements

efficiency improvements should be possible. In addition, of course, tests and mathematical analyses of the method should be performed. While these research tasks still require significant effort, we do believe that the MFS has an excellent potential for applications in solid and fluid mechanics.

**Appendix A**  
**Cubature on annular sectors in  $R^2$**

In this appendix we state without proof a product cubature rule for the integral

$$\iint_{\Omega} f(x, y) dx dy \doteq \sum_i \sum_j D_{ij} f(x_i, y_j) \tag{34}$$

with an accuracy of  $k$ . The region under consideration is the annular sector with inner radius  $R_i$  and outer radius  $R_o$  and angular span of  $(-\theta_o, \theta_o)$  (see Fig. A1). The dot over the equality signifies that the relationship is a strict equality if the function  $f(x, y)$  is a polynomial of order at most  $k$  in  $x$  and  $y$ , otherwise it is an approximation.

**Cubature Rule** If it is required that the rule in Eq. 34 have accuracy  $k = 4m + 3$ ,  $m = 0, 1, 2, \dots$ , in  $x = r \cos \theta$  and  $y = r \sin \theta$ , and if it is required to have a minimum number of evaluation points which are taken at the intersection of concentric arcs (radius  $r_j$ ) with rays emanating from the origin (angle  $\theta_i$ ), then it is both necessary and sufficient for the existence of a unique set of weights  $D_{ij} \in R$  that the following two conditions be satisfied:

1. Let  $z_\alpha$  be the  $(k + 1)/2$  zeros of the polynomial  $\pi_p(z)$  of degree  $p = (k + 1)/2$  which is orthogonal to all polynomials of inferior degree on  $[-1, 1]$  relative to the weight

$$w(z) = (1 + z)^{-\frac{1}{2}} \left( \frac{3 + \cos \theta_o}{1 - \cos \theta_o} - z \right)^{-\frac{1}{2}} .$$

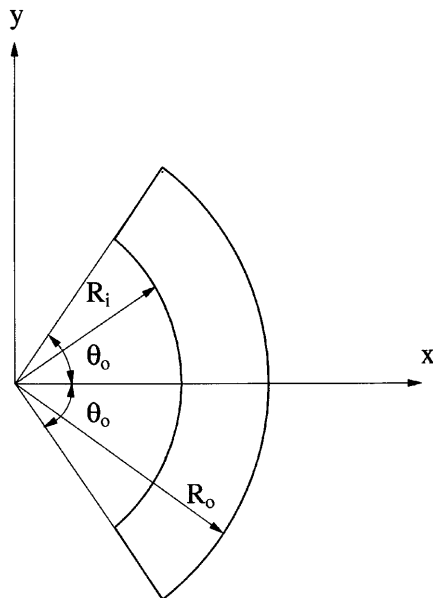


Fig. A1. A sector on which the cubature rule in Appendix A is developed

Let angular positions  $\varphi_\alpha$  be defined by the following relationship

$$\cos \varphi_\alpha = \left( \frac{1 + \cos \theta_o}{2} \right) - \left( \frac{1 - \cos \theta_o}{2} \right) z_\alpha$$

$$\alpha = 1, 2, \dots, (k + 1)/2 .$$

Then the  $(k + 1)$  angular positions  $\theta_i$  of the evaluation points are given by

$$\theta_i = \begin{cases} \varphi_i & i = 1, 2, \dots, (k + 1)/2 \\ -\varphi_{i-(k+1)/2} & i = (k + 3)/2, \dots, (k + 1) \end{cases}$$

2. The radial positions of the evaluation points  $r_j$  are the positive square roots of the  $m + 1$  zeros of  $P_{m+1}(r^2)$ , the Legendre polynomial in  $r^2$  of degree  $m + 1$ , orthogonalized on  $[R_i^2, R_o^2]$ .

The (unique) weights  $D_{ij}$  are equal to  $A_i B_j$ , where

$$A_i = \begin{cases} \int_{-1}^1 w(\xi) [l_i(\xi)]^2 d\xi & i = 1, 2, \dots, (k + 1)/2 \\ \int_{-1}^1 w(\xi) [l_{i-(k+1)/2}(\xi)]^2 d\xi & i = (k + 3)/2, \dots, (k + 1) \end{cases}$$

and

$$B_j = \frac{1}{2P'_{m+1}(r_j^2)} \int_{R_i^2}^{R_o^2} \frac{P_{m+1}(r^2)}{r^2 - r_j^2} dr^2 \quad j = 1, 2, \dots, m + 1 .$$

The functions  $l_i(z)$  being given as

$$l_i(z) = \frac{\pi_p(z)}{(z - z_i) \pi'_p(z_i)} .$$

An important corollary of this rule is the case when  $\theta_o = \pi$ , i.e. when we have internal disks or annuli. The complicated polynomial  $\pi_p(z)$  in the above rule reduces to the well known Chebyshev polynomial of the first kind and the quantities  $\theta_i$  and  $A_i$  are known in closed form. We state the corollary formally:

**Corollary A.1** For the special case of  $\theta_o = \pi$ , the above theorem yields the following cubature rule

$$\iint_{\Omega} f(x, y) dx dy \doteq \sum_{i=1}^{4(m+1)} \sum_{j=1}^{m+1} C_j f(r_j \cos \theta_i, r_j \sin \theta_i) ,$$

where

1.  $\theta_i = (i\pi)/(2(m + 1))$  ,
2.  $C_j = \frac{1}{(4(m+1)P'_{m+1}(r_j^2))} \int_{R_i^2}^{R_o^2} \frac{P_{m+1}(r^2)}{(r^2 - r_j^2)} dr^2$  ,
3.  $P_{m+1}(r^2)$  is the Legendre polynomial in  $r^2$  of degree  $m + 1$ , orthogonalized on  $[R_i^2, R_o^2]$ .
4.  $P_{m+1}(r_j^2) = 0$ .

The case  $\theta_o = \pi$  has been previously derived by Peirce (1957a).

**References**

Atluri SN, Kim H, Cho JY (1999a) A critical assessment of the truly meshless local Petrov-Galerkin (MLPG), and local boundary integral equation (LBIE) methods. *Comput. Mech.*, in press

- Atluri SN, Cho JY, Kim H (1999b)** Analysis of thin beams, using the meshless local Petrov-Galerkin method, with generalized moving least squares interpolations. *Comput. Mech.*, accepted for publication.
- Atluri SN, Zhu T (1998a)** A new meshless local Petrov-Galerkin (MLPG) approach in computational mechanics. *Comput. Mech.* 22:117–127
- Atluri SN, Zhu TL (1998b)** A new meshless local Petrov-Galerkin (MLPG) approach to nonlinear problems in computer modeling and simulation. *Comp. Mod. Simul. Eng.* 3(3): 187–196
- Babuška I, Melenk JM (1997)** The partition of unity method. *Int. J. Num. Meth. Eng.* 40:727–758
- Bathe KJ (1996)** *Finite Element Procedures*. Prentice Hall, Englewood Cliffs, NJ
- Belytschko T, Lu YY, Gu L (1994)** Element free Galerkin methods. *Int. J. Num. Meth. Eng.* 37:229–256
- Belytschko T, Krongauz Y, Organ D, Fleming M, Krysl P (1996)** Meshless methods: an overview and recent developments. *Comp. Meth. Appl. Mech. Eng.* 139:3–47
- Dolbow J, Belytschko T (1999)** Numerical integration of the Galerkin weak form in meshfree methods. *Comput. Mech.* 23:219–230
- Duarte CA, Oden JT (1996a)** *H-p* clouds – an *h-p* meshless method. *Num. Meth. Partial Differential Equations* 12: 673–705
- Duarte CA (1995)** A review of some meshless methods to solve partial differential equations. TICAM Report 95-06, TICAM, The University of Texas at Austin
- Duarte CA, Oden JT (1996b)** An *h-p* adaptive method using clouds. *Comp. Meth. Appl. Mech. Eng.* 139:237–262
- Duarte CA, Babuška I, Oden JT (1999)** Generalized finite element methods for three dimensional structural mechanics problems. *Com. Struct.*, submitted for publication
- Günther FC, Liu WK (1998)** Implementation of boundary conditions for meshless methods. *Comp. Meth. Appl. Mech. Eng.* 163:205–230
- Krongauz Y, Belytschko T (1996)** Enforcement of essential boundary conditions in meshless approximations using finite elements. *Comp. Meth. Appl. Mech. Eng.* 131:133–145
- Lether FG (1971)** A generalized product rule for the circle. *SIAM J. Num. Anal.* 8(2):249–253
- Li S, Liu WK (1999a)** Reproducing kernel hierarchical partition of unity, part I – formulation and theory. *Int. J. Num. Meth. Eng.* 45:251–288
- Li S, Liu WK (1999b)** Reproducing kernel hierarchical partition of unity, part II – applications. *Int. J. Num. Meth. Eng.* 45: 289–317
- Liu WK, Li S, Belytschko T (1997)** Moving least-square reproducing kernel methods, part I: methodology and convergence. *Comp. Meth. Appl. Mech. Eng.* 143:113–154
- Li S, Liu WK (1996)** Moving least-square reproducing kernel method, part II: Fourier analysis. *Comp. Meth. Appl. Mech. Eng.* 139:159–193
- Liu WK, Adee J, Jun S (1993)** Reproducing kernel particle methods for elastic and plastic problems. In: Benson DJ, Asaro RA (eds.) *Advanced Computational Methods for Material Modeling*, AMD 180 and PVP 33, ASME pp. 175–190
- Lu YY, Belytschko T, Gu L (1994)** A new implementation of the element free Galerkin method. *Comp. Meth. Appl. Mech. Eng.* 113:397–414
- Melenk JM (1992)** Finite element methods with harmonic shape functions for solving Laplace’s equation. Master of Arts Thesis, University of Maryland
- Melenk JM, Babuška I (1996)** The partition of unity finite element method: basic theory and applications. *Comp. Meth. Appl. Mech. Eng.* 139:289–314
- Melenk JM, Babuška I (1997)** Approximation with harmonic and generalized harmonic polynomials in the partition of unity method. *Comp. Assisted Mech. Eng. Sci.* 4:607–632
- Monaghan JJ (1988)** An introduction to SPH. *Comp. Phys. Comm.* 48:89–96
- Nayroles B, Touzot G, Villon P (1992)** Generalizing the FEM: diffuse approximation and diffuse elements. *Comput. Mech.* 10:307–318
- Pearce WH (1957a)** Numerical integration over the planar annulus. *J. Soc. Ind. App. Math.* 5(2):66–73
- Pearce WH (1957b)** Numerical integration over the spherical shell. *Math. Tables and Other Aids to Computation* 11(60):244–249
- Oden JT, Duarte CA, Zienkiewicz OC (1998)** A new cloud-based *hp* finite element method. *Comp. Meth. Appl. Mech. Eng.* 153:117–126
- Oñate E, Idelsohn S, Zienkiewicz OC, Taylor RL (1996)** A finite point method in computational mechanics. Applications to convective transport and fluid flow. *Int. J. Num. Meth. Eng.* 39:3839–3866
- Shepard D (1968)** A two-dimensional interpolation function for irregularly spaced data. *Proc. 23rd Nat. Conf. ACM* 517–524
- Stoyanova S (1997)** Cubature formulae of the seventh degree for the hypersphere. *J. Comp. Appl. Math.* 84:15–21
- Stroud AH (1971)** *Approximate Calculation of Multiple Integrals*. Prentice-Hall, Englewood Cliffs, NJ
- Wagner GJ, Liu WK (1999)** Application of essential boundary conditions in mesh-free methods: a corrected collocation method. *Int. J. Num. Meth. Eng.*, submitted for publication
- Washizu K (1975)** *Variational Methods in Elasticity and Plasticity*. 2nd Edn., Pergamon Press, New York
- Yosida K (1978)** *Functional Analysis*. 5th Edn., Springer-Verlag, Berlin Heidelberg
- Zhu T, Atluri SN (1998a)** A modified collocation method and a penalty formulation for enforcing the essential boundary conditions in the element free Galerkin method. *Comput. Mech.* 21:211–222
- Zhu T, Zhang JD, Atluri SN (1998b)** A local boundary integral equation (LBIE) method in computational mechanics and a meshless discretization approach. *Comput. Mech.* 21:223–235